

illuminating the Hidden: Standardizing Cardiac MIBG Imaging for Sympathetic Dysfunction

Justin G. Peacock*^{1,2}, Haley Majot³, Avani T. Bansal⁴, Patrick Neshiwat⁵, Kelsy Dimeff¹, and Kalpna Prasad*¹

¹Department of Radiology, Walter Reed National Military Medical Center, Bethesda, Maryland; ²Department of Radiology, Uniformed Services University, Bethesda, Maryland; ³Department of Radiology, Geisinger Medical Center, Danville, Pennsylvania; ⁴The Potomac School, The Science and Engineering Research Center, McLean, Virginia; and ⁵Department of Cardiology, Hartford Hospital, Hartford, Connecticut

CE credit: For CE credit, you can access the test for this article, as well as additional JNMT CE tests, online at <https://www.snmlearningcenter.org>. You may make 3 attempts to pass the test and must answer 80% of the questions correctly to receive credit—number of credits awarded will be determined by the length of the article. Participants can access this activity through the SNMMI website (<http://www.snmlearningcenter.org>) through June 2028. Additional details such as the number of credits issued per article, expiration dates, financial disclosure information, VOICE transcripts, and the process to earn CE credit can also be found in the SNMMI Learning Center.

The heart's innervation relies on a delicate balance between the sympathetic and parasympathetic nervous systems, each using distinct neurotransmitters to regulate heart rate, contractility, and vascular tone. The sympathetic division primarily uses norepinephrine, whereas the parasympathetic division operates through acetylcholine. A range of diseases, through intrinsic and extrinsic mechanisms, can disrupt these neural pathways, resulting in autonomic dysfunction. This review highlights intrinsic causes such as dysautonomias, amyloidosis, diabetes mellitus, Parkinsonian syndromes, and Lewy body dementia, as well as extrinsic factors such as heart failure, myocardial ischemia, infarction, and drug-induced cardiotoxicity. This article examines the effects of various conditions on cardiac sympathetic innervation and highlights how ¹²³I-radiolabeled metaiodobenzylguanidine (MIBG), a norepinephrine analog, can target the cardiac sympathetic nervous system for early detection and disease characterization. Currently, variability in cardiac ¹²³I-MIBG imaging protocols across institutions leads to inconsistencies in image acquisition and interpretation, limiting the establishment of universal benchmarks for distinguishing normal from abnormal cardiac sympathetic innervation. To address this, we propose a simple, clinically useful, standardized protocol based on European Association of Nuclear Medicine guidelines and the AdreView Myocardial Imaging for Risk Evaluation in Heart Failure trial, incorporating both qualitative and semiquantitative methods for disease assessment and highlight cutoff values for some pathologies that can assist in visual interpretation. Standardizing these protocols will enhance the consistency, reliability, and diagnostic accuracy of ¹²³I-MIBG imaging, improving clinical decision-making and optimizing patient outcomes.

Key Words: cardiac ¹²³I-MIBG; sympathetic nervous system imaging; cardiac autonomic dysfunction; dysautonomia

J Nucl Med Technol 2025; 00:1–11

DOI: 10.2967/jnmt.124.269436

Received Dec. 27, 2024; revision accepted Mar. 18, 2025.
For correspondence or reprints, contact Justin Peacock (justin.peacock@usuhs.edu) or Kalpna Prasad (kalpna.prasad.civ@health.mil).
*Contributed equally to this work.
Published online Apr. 22, 2025.
COPYRIGHT © 2025 by the Society of Nuclear Medicine and Molecular Imaging.

ANATOMY AND PHYSIOLOGY OF CARDIAC INNERVATION

The heart is innervated by the autonomic nervous system, comprising the sympathetic and parasympathetic systems, which regulate chronotropy, lusitropy, dromotropy, and inotropy (1). Sympathetic nerves release catecholamines such as norepinephrine to stimulate adrenergic receptors, increasing heart rate and contractility, whereas parasympathetic nerves release acetylcholine to stimulate muscarinic receptors, decreasing heart rate and contractility (1–5). Sympathetic signals originate in the brain, travel through the spinal cord, and exit at T1–T4, synapsing with postganglionic fibers near the vertebral column that primarily target the ventricles (Fig. 1) (1,3). Parasympathetic fibers originate in the medulla, traverse the vagus nerve, and synapse within the heart, mainly innervating the atria to regulate nodal function (Fig. 1) (1,3).

Norepinephrine, derived from tyrosine, is synthesized and stored in presynaptic vesicles at high concentrations (Fig. 2) (3,4,6). On stimulation, it is released into the synaptic space, binding to α -1, β -1 (the primary cardiac adrenergic receptor), and β -2 receptors on cardiac myocytes, increasing heart rate and contractility (4,7). Most norepinephrine is recycled and stored via the norepinephrine uptake-1 pathway or catabolized (3). This pathway helps regulate synaptic norepinephrine levels, preventing excessive catecholamine effects on the heart (Fig. 2).

CARDIAC AUTONOMIC DYSFUNCTION

Cardiac sympathetic dysfunction can arise from intrinsic nerve abnormalities or external disease processes, leading to neurohormonal imbalances, myocyte damage, or sympathetic denervation (1,3,4,8,9). Regardless of the cause, this dysfunction results in systemic dysautonomia, manifesting as heart rate irregularities, blood pressure instability, arrhythmias,

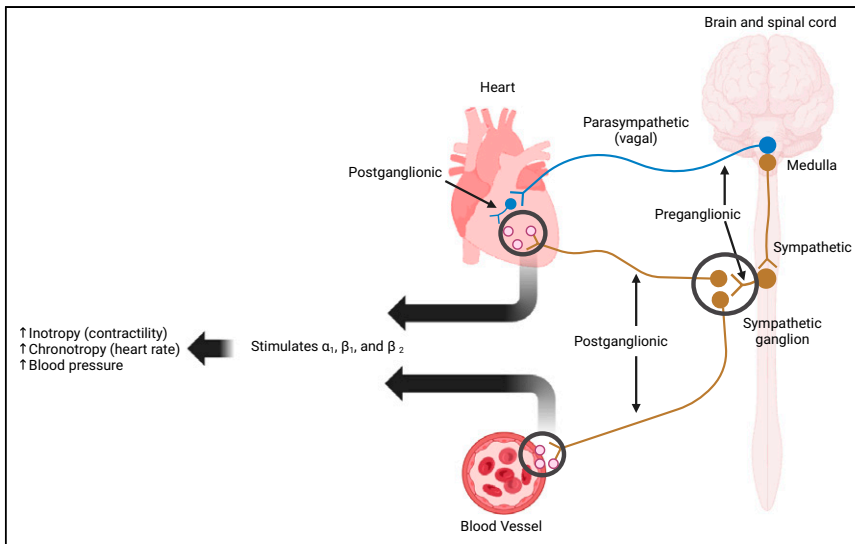


FIGURE 1. Sympathetic (brown) and parasympathetic (blue) innervation of heart and systemic vasculature. Postganglionic sympathetic neurons are seen innervating heart and systemic vasculature.

and impaired diastolic relaxation (1). We will discuss the following intrinsic and extrinsic causes of cardiac sympathetic dysfunction.

Intrinsic Mechanisms

Dysautonomias. Dysautonomia, or autonomic dysfunction, encompasses congenital and acquired disorders that disrupt autonomic functions such as blood pressure,

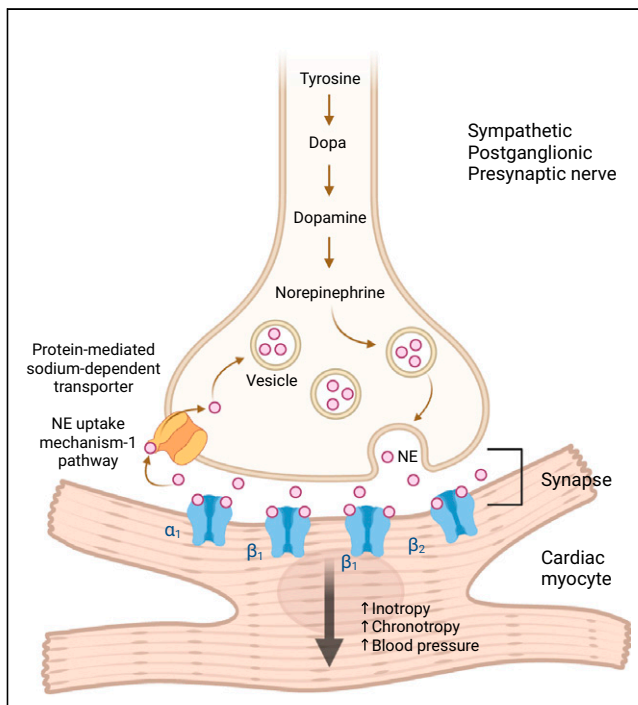


FIGURE 2. Diagram of sympathetic neuronal synapse with cardiac myocyte, demonstrating norepinephrine (NE) synthesis, storage, release, and reuptake.

temperature regulation, breathing, and heart rate (9–11). Its diverse symptoms complicate diagnosis and treatment. Dysautonomia exists in primary (inherited or idiopathic) and secondary forms. Primary dysautonomia has been observed in Ashkenazi Jewish and Eastern European populations (10). Secondary dysautonomia arises from systemic conditions such as amyloidosis, Parkinsonian syndromes, malignancies, and inflammatory diseases, including long coronavirus disease 2019 (10,11).

Amyloidosis. Amyloidosis involves misfolded protein aggregates infiltrating organs, including the heart, leading to a poor prognosis with risks of heart failure, arrhythmias, and restrictive cardiomyopathy (12–14). It also causes dysautonomia due to sympathetic denervation and conduction tissue infiltration. Cardiac dysautonomia is most common in hereditary transthyretin-related (ATTR) and immunoglobulin light chain amyloidosis but not in wild-type or senile ATTR (13).

Diabetes Mellitus. Diabetes mellitus is a common cause of intrinsic cardiac autonomic dysfunction, though its exact pathology remains unclear (1,3,6,15–19). It leads to autonomic denervation, primarily affecting distal axons, through mechanisms such as glycosylation and ischemia (1). Although parasympathetic involvement has been demonstrated, its impact on sympathetic signaling is complex (1).

Parkinsonian Syndromes. Parkinsonian syndromes are neurologic disorders characterized by dopaminergic neuron degeneration, including Parkinson disease (PD), multiple system atrophy (MSA), progressive supranuclear palsy, corticobasal syndrome, and dementia with Lewy bodies (DLB) (20). In addition to neuron loss, some syndromes exhibit cardiac dysautonomia and sympathetic denervation (21). MSA affects preganglionic neurons, preserving cardiac sympathetic innervation, whereas PD impacts postganglionic neurons, leading to cardiac sympathetic denervation (21–23).

Extrinsic Mechanisms

Heart Failure. Heart failure, most commonly caused by ischemia, leads to neurohormonal dysregulation, activating the renin–angiotensin and sympathetic nervous systems (1,4). This triggers oxidative stress in the brain, increasing catecholamine levels that deplete norepinephrine storage, reduce adrenergic receptor expression, and impair norepinephrine reuptake (4). The resulting sympathetic synapse dysfunction leads to excessive catecholamine levels, eventually becoming cytotoxic.

Myocardial Ischemia or Infarction. Cardiac sympathetic nerves are highly susceptible to ischemia and can undergo denervation after chronic ischemia or infarction (1,3,6,24).

Denervation occurs at and around the infarct site, alongside ventricular remodeling (3). Similar to heart failure, neurohormonal changes lead to elevated catecholamine levels, depleted presynaptic norepinephrine storage, reduced norepinephrine transporter activity, and decreased postsynaptic adrenergic receptor expression, resulting in dysfunctional sympathetic synapses (3).

IMAGING WITH ^{123}I -METAIODOBENZYLGUANIDINE (MIBG)

MIBG is a guanethidine analog taken up by sympathetic adrenergic neurons and chromaffin cells (6,25). Labeled with ^{123}I , a pure γ -emitter, it can be imaged using γ -cameras. Structurally similar to norepinephrine (Fig. 3), ^{123}I -MIBG shares its release, reuptake, and storage mechanisms but has no physiologic effect on postsynaptic receptors (Fig. 4). ^{123}I -MIBG was initially developed in the early 1970s to image the adrenal medulla and later to detect pheochromocytoma, neuroendocrine tumors, neuroblastoma, and, to a lesser extent, carcinoid, medullary thyroid carcinoma, and paraganglioma (25–27). Normally, it is distributed in sympathetic-innervated areas, including the salivary glands, thyroid, heart, liver, spleen, adrenal glands, kidneys, and bladder (28). Stored in presynaptic sympathetic vesicles without being catabolized, ^{123}I -MIBG uptake in the heart should be significantly higher than in the mediastinum (Fig. 4) (29). Reduced uptake indicates sympathetic denervation or dysfunction; these conditions also accelerate its washout (Fig. 5). Thus, ^{123}I -MIBG imaging quantifies cardiac sympathetic dysfunction by measuring decreased uptake and increased washout.

Cardiac ^{123}I -MIBG Scanning

Significant protocol and image analysis variation in the literature limits widespread clinical applicability of cardiac ^{123}I -MIBG imaging (30,31). Standardization of ^{123}I -MIBG imaging and analysis is required for comparison of results across different institutions, interreader reliability, ordering provider confidence in the results, and insurance reimbursement. Studies on cardiac ^{123}I -MIBG imaging demonstrate variability in the imaging technique (planar/SPECT), collimators (low-energy, high resolution/medium energy), planar image projections (anterior/left anterior oblique), image timing (varying early and delayed time points), and analytic measurements (semiquantitative SPECT values, heart-to-mediastinum ratios [HMR], and washout rates [WRs]), among other parameters (3,30,31). The most widely used

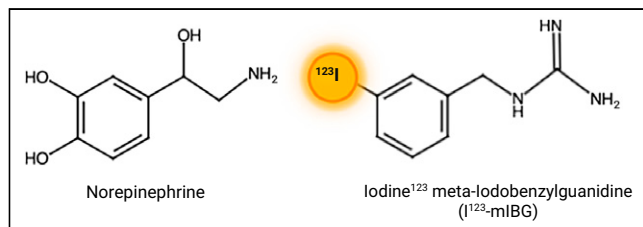


FIGURE 3. Chemical structure of norepinephrine and norepinephrine radiolabeled with ^{123}I -MIBG.

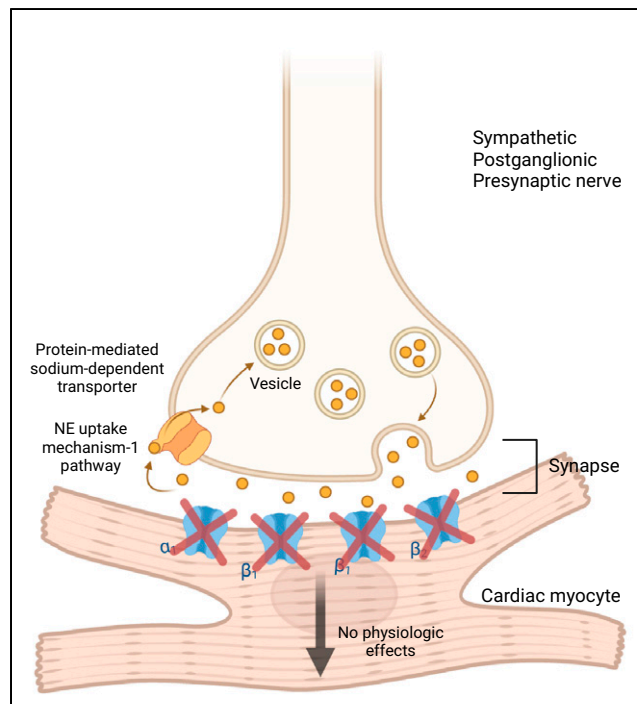


FIGURE 4. Sympathetic postganglionic presynaptic nerve synapsing with cardiac myocyte. ^{123}I -MIBG uptake at synapse mimics norepinephrine (NE) reuptake and does not bind to adrenergic receptors on myocyte membrane nor result in downstream sympathetic effects.

protocol in the literature is similar to that proposed by the European Association of Nuclear Medicine (EANM) Cardiovascular Committee and the European Council of Nuclear Cardiology in 2010 (30). The large, multicenter, prospective AdreView Myocardial Imaging for Risk Evaluation in Heart Failure (ADMIRE-HF) trial that used cardiac ^{123}I -MIBG imaging for risk assessment in heart failure patients used a similar protocol with planar and SPECT imaging (32). Primarily using the EANM proposal and methods from the ADMIRE-HF trial, we share the imaging protocol used clinically in our institution with an attempt to offer a simplified procedure and image interpretation for ^{123}I -MIBG scans (30,32–35).

Indications and Contraindications

Cardiac ^{123}I -MIBG imaging evaluates sympathetic innervation, aiding in diagnosing and assessing cardiac dysautonomia causes such as systemic dysautonomia, amyloidosis, diabetes, Parkinsonian syndromes, heart failure, and ischemic heart disease (Table 1) (3). The scan is contraindicated in patients with known hypersensitivity to MIBG/MIBG sulfate (Table 1). Its safety in neonates under 1 mo is unestablished, and the benzyl alcohol in ^{123}I -MIBG preparations poses additional risks in neonates, including gasping syndrome, hypotension, metabolic acidosis, and kernicterus (35). Patients with severe renal impairment or those on dialysis require special consideration, as ^{123}I -MIBG is renally excreted but not cleared by dialysis (30). This can lead to prolonged radiation

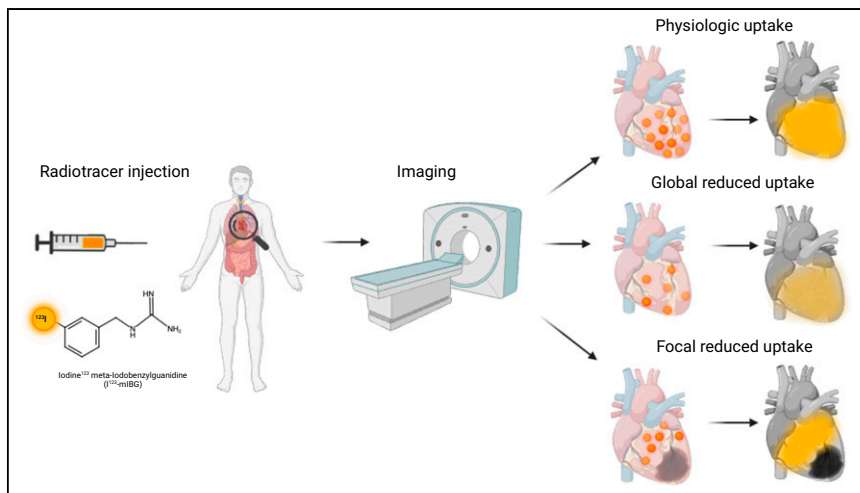


FIGURE 5. After injection of ^{123}I -MIBG (yellow), patient undergoes imaging with 3 generalized outcomes. Normal physiologic uptake signifies global radiotracer distribution throughout heart's sympathetic regions significantly more than background mediastinal activity. Globally decreased (lighter yellow) or focally absent uptake (black) signifies conditions with abnormally reduced sympathetic innervation, such as PD or heart failure. Lastly, focally decreased uptake can be observed in conditions causing localized defects in sympathetic innervation, such as ischemic infarcts.

exposure and increased background activity, potentially impairing scan quality and diagnostic accuracy.

Patient Information and Preparation

Patients may have concerns about radiation exposure and should receive written instructions covering the procedure, benefits, risks, preparation, and postscan guidelines (Table 1). Reassurance on radiation exposure to others and methods to minimize it for themselves should be provided. The following patient preparation items, detailed in Tables 1 and 2, are particularly pertinent:

- Certain medications interfere with ^{123}I -MIBG uptake and may need to be withheld, whereas essential cardiac medications may be continued if necessary (Table 2) (29,30,36–38).
- Foods containing vanillin or catecholaminelike compounds (e.g., chocolate, blue cheese) should be avoided before the scan (39).
- Pregnancy and lactation should be assessed, as ^{123}I crosses the placenta and is excreted in breast milk. Breastfeeding should be discontinued for at least 48 h, with the package insert suggesting up to 6 d to minimize risk (30,35).
- To protect the thyroid, iodine or perchlorate medications should be administered before the scan (36,40,41).
- Patients with a prior thyroidectomy do not need thyroid blocking.
- Hydration and frequent voiding help reduce bladder radiation exposure, as ^{123}I -MIBG is excreted primarily through the kidneys and is not cleared by dialysis (30). Patients with severe renal impairment require special consideration because of prolonged radiation exposure.

Radiopharmaceutical Administration

An activity of 10 mCi (370 MBq) of ^{123}I -MIBG should be administered via standard slow intravenous injection over 1–2 min for patients 16 y or older or for patients weighing 70 kg or more if less than 16 y of age (Table 1)

(30,35,37). For pediatric patients younger than 16 y and weighing less than 70 kg, the North American Consensus Guidelines' recommended activity is 0.14 mCi/kg (5.2 MBq/kg) with a minimum recommended activity of 1 mCi (37 MBq), whereas the EANM pediatric guidelines are slightly higher (42,43). The radiopharmaceutical injection should be followed by an injection of 0.9% sodium chloride to ensure complete radiopharmaceutical delivery.

Image Acquisition

Assessment of uptake can be obtained with early (10–15 min) and delayed (3 h 50 min or 4 h) anterior planar imaging for 10 min each (Table 3) (29,30,32–34). The delayed time point not only incorporates neuronal integrity seen in the early images but also incorporates the complete neuronal functioning of norepinephrine uptake, storage in

vesicles, and release and reuptake mechanism. At our institution, because of the delayed image advantages and consistent results, we only perform delayed imaging.

A γ -camera with a large field of view should be used. The collimators should be low-energy, high-resolution, parallel hole collimators (Table 3). Energy windows should be centrally set at 20%, with the window centered at a 159-keV photopeak. A preferable planar image matrix of 256×256 is used if possible, but a 128×128 matrix may be used if a higher resolution is not available (29).

The patient should be in the supine position, with female patients imaged without a bra. SPECT with or without CT should be performed for adequate visual assessment and to avoid any confounding ^{123}I -MIBG activity on anterior planar images. SPECT images also eliminate the need for lateral planar images. SPECT images are performed with a patient's arms elevated above the head.

Image Processing and Quantification

Cardiac ^{123}I -MIBG uptake is assessed using the HMR, calculated from counts per pixel in regions of interest (ROI). Although both early and delayed images can be used, delayed HMR is preferred because of reduced confounding from blood pool uptake and more consistent results. This approach aligns with the ADMIRE-HF trial, which used delayed HMR for primary analysis (32). Normal delayed uptake indicates intact postganglionic sympathetic innervation (44).

For HMR calculation, the anterior projection is used, with an ROI drawn over the heart. Some protocols contour the myocardium precisely, whereas others encompass the entire heart to reduce variability (45). This method also simplifies the process for technologists, particularly in cases in which low or absent uptake makes delineation of the ventricular wall

TABLE 1
¹²³I-MIBG Cardiac Scintigraphy Provider Summary and Protocol

Indication	Contraindication and precaution	Patient preparation and education	Radiopharmaceutical, dose, and administration
<p>Evaluation of cardiac sympathetic innervation</p>	<p>Known hypersensitivity to iobenguane or iobenguane sulfate</p> <p>Risk of serious reactions in infants due to benzyl alcohol preservative: neonates and infants can experience serious and fatal adverse reactions, including “gasping syndrome” with benzyl alcohol-preserved drugs such as current commercially available ¹²³I-MIBG in the United States (AdreView)</p>	<p>When medically feasible, withhold drugs known to interfere with uptake of ¹²³I-MIBG</p> <p>Nursing mothers should pump and discard breast milk for 6 d after ¹²³I-MIBG administration to minimize the risk to nursing infants</p>	<p>¹²³I-MIBG</p> <p>Activity:</p> <ul style="list-style-type: none"> Adults ≥16 y or children <16 y and ≥70 kg is 10 mCi (370 MBq) Children <16 y and <70 kg is 0.14 mCi/kg (5.2 MBq/kg) Minimum recommended activity is 1 mCi (37 MBq)
<p>No appropriate use criteria have been developed to date for cardiac ¹²³I-MIBG scans</p>	<p>Severe renal impairment can cause increased radiation exposure due AdreView clearance by glomerular filtration and nondialyzable property</p> <p>Pregnancy: radioactive iodine can cross the placenta and permanently impair fetal thyroid function, causing fetal harm; do not administer to pregnant women</p>	<p>Patients should stop eating food containing vanillin and catecholamine-like compounds (e.g., chocolate and blue cheese) for approximately 1 wk prior</p> <p>Pretreatment with potassium iodine given orally at least 1 h before injection of the radiopharmaceutical:</p> <ul style="list-style-type: none"> Adult dose: 130 mg of potassium iodide (2 drops or 0.13 mL of saturated solution of potassium iodide) in 1 ounce = 30 mL of distilled water Pediatric Dose: <ul style="list-style-type: none"> 1–36 mo: 42.5 mg of potassium iodate 3–12 y: 85 mg of potassium iodate Above 12 y old: 170 mg of potassium iodate Alternative is potassium perchlorate (400 mg for adults, body weight-adjusted for children) 	<p>Technique of administration:</p> <ul style="list-style-type: none"> Standard slow intravenous injection over 1–2 min
<p>Lactation: ¹²³I is present in breast milk, and there is no information on its effect on breastfed infants</p>	<p>Pediatric use: safety and effectiveness have not been established in newborns <1 mo old or in any pediatric patients with congestive heart failure</p>		

TABLE 2
Common Drugs Affecting ¹²³I-MIBG Uptake

Drug group	Drug name	Withdrawal time	Mechanism of action
Adrenergic neuron blockers	Guanethidine, reserpine	48 h	2, 3
α-blockers	Phenoxybenzamine (intravenous doses)	15 d	5
Antiarrhythmics for ventricular arrhythmias	Amiodarone	Not practical to withdraw	1, 3
Antipsychotics (neuroleptics)	Chlorpromazine	24 h	1
Antipsychotics (neuroleptics)	Fluphenazine	24 h or 1 mo for depot	1
Antipsychotics (neuroleptics)	Haloperidol	48 h or 1 mo for depot	1
β ₂ stimulants	Salmeterol, salbutamol	24 h	3
Calcium channel blockers	Diltiazem, nifedipine	24 h	4
Calcium channel blockers	Felodipine, amlodipine, nicardipine, verapamil	48 h	4
Combined α- and β-blocker	Labetalol	72 h	1, 3
Cocaine		7–14 d	1
Inotropic sympathomimetics	Dobutamine, dopamine	24 h	3
Opioid analgesics	Tramadol	24 h	1
Opioid		7–14 d	
Sedating antihistamines	Promethazine	24 h	1
Sympathomimetics for glaucoma	Brimonidine	48 h	3
Systemic and local nasal decongestants	Pseudoephedrine, phenylephrine	48 h	3
Systemic and local nasal decongestants	Ephedrine	24 h	1
Antipsychotics (neuroleptics)	Clozapine	7 d	1
Antipsychotics (neuroleptics)	Olanzapine	7 – 10 d	1
Antipsychotics (neuroleptics)	Quetiapine	48 h	1
Antipsychotics (neuroleptics)	Risperidone	5 d or 1 mo for depot	1
Tricyclic antidepressants	Imipramine, nortriptyline, doxepin	24 h	1
Tricyclic antidepressants	Amitriptyline	48 h	1
Tricyclic-related antidepressants	Venlafaxine	48 h	1
Tricyclic-related antidepressants	Mirtazapine	8 d	1
Vasoconstrictor sympathomimetics	Norepinephrine	24 h	3

Table adapted from articles reviewing the practical aspects of ¹²³I-MIBG imaging (30,36,37). Mechanism of action 1: inhibition of norepinephrine uptake mechanism-1 pathway. Mechanism of action 2: inhibition of uptake by active transport into vesicles. Mechanism of action 3: depletion of granules. Mechanism of action 4: increased uptake and retention.

challenging on planar images. In our practice, we typically use a circular ROI encompassing the entire heart or a freehand ROI to match its shape, calculating mean counts per pixel.

For the mediastinum, conventional 7 × 7 pixel ROI placement on a 128 × 128 matrix can be cumbersome because of patient variability and software limitations (35,37). Instead, we use a longitudinal rectangular ROI in the midline mediastinum at least 4 pixels below the clavicular heads, avoiding the thyroid, muscles, lungs, or abnormal MIBG activity (Fig. 6). This ensures placement in the area with the lowest background counts, from which the mean mediastinal counts per pixel are calculated. The HMR is then determined by dividing mean myocardial counts by mean mediastinal counts, providing a key semiquantitative measure of myocardial sympathetic innervation:

$$\text{HMR} = \text{H/M} = \frac{\text{Mean heart value (counts per pixel)}}{\text{Mean mediastinal value (counts per pixel)}}$$

Myocardial WR reflects nerve integrity and sympathetic drive, mainly representing the norepinephrine uptake-1 mechanism (44). Cardiac disorders increase sympathetic activity and decrease norepinephrine reuptake, causing higher ¹²³I-MIBG washout and decreased delayed cardiac uptake. The WR is calculated as the percentage decrease in myocardial radiotracer from early to delayed images, normalized to mediastinal activity (Fig. 7):

$$\text{WR (\%)} = \frac{\left[\begin{array}{l} \text{(early cardiac uptake - early mediastinal uptake)} \\ - \left(\begin{array}{l} \text{delayed cardiac uptake} \\ - \text{delayed mediastinal uptake} \end{array} \right) \end{array} \right]}{\text{}} \cdot 100$$

SPECT Reconstruction

SPECT or SPECT/CT imaging improves contrast resolution and should be performed to better visualize uptake in

TABLE 3
¹²³I-MIBG Scintigraphy Imaging Parameters

Parameter	Characteristic	Standard/preferred/optional
Camera type	Large-field-of-view γ -camera	Standard
Energy peak	159 keV	Standard
Energy window	20%	Standard
Collimator	Low-energy, high resolution, parallel hole	Standard
Patient position	Supine	Standard
Field of view	Heart/chest	Standard
Injection-to-imaging time (delayed images)	Late images at 3 h 50 min	Standard
Planar		Standard
Acquisition type	Static	Standard
Detector configuration	180°	Standard
Views	Anterior and lateral	Standard
Number of views	2	Standard
Counts/time per view	10 min per image	Standard
Matrix	256 × 256 (minimum 128 × 128)	Standard
Magnification	Zoom = 1	Standard
SPECT or SPECT/CT		Optional
Acquisition type	Step and shoot	Optional
Patient position	Supine	Optional
Orbit	360°	Optional
Matrix	128 × 128	Optional
Magnification	Zoom = 1	Optional
Pixel size	Per camera settings	Optional
Projections per detector	120 steps (60 steps/detector)	Optional
Time per projection	30 s per step	Optional
CT attenuation correction	Standard attenuation correction	Optional
CT parameters	120 kV, 25 mA, pitch = 1.25	Optional
CT parameters	Slice thickness, 2.5 mm; 1 s/rotation	Optional

the myocardium (3,31,46). Additionally, SPECT imaging can provide segmental analysis of ¹²³I-MIBG uptake throughout the left ventricle. Segmental analyses in the literature use a semiquantitative technique on 5–20 segments, commonly scoring 0–3 or 0–4 for each segment (0 represents

normal uptake and 3 or 4 represent absent uptake) (47,48). These scores can be summed for the left ventricle and correlated with disease pathology. For example, a summed score of 26 or greater on delayed SPECT imaging was shown to predict implantable cardioverter-defibrillator therapy appropriateness and cardiac death among heart failure patients (3). Further work on SPECT-delayed summed-score cutoffs needs to be conducted for a variety of cardiac pathologies to determine the optimal prognostic scores.

For SPECT imaging, we use a dual head camera, 128 × 128 matrix with a 360° orbit and 180° acquisition starting at 45° right anterior oblique and proceeds counterclockwise to 45° left posterior oblique. We use 120 steps (60 steps per detector) and 30 s per step. No gating is performed.

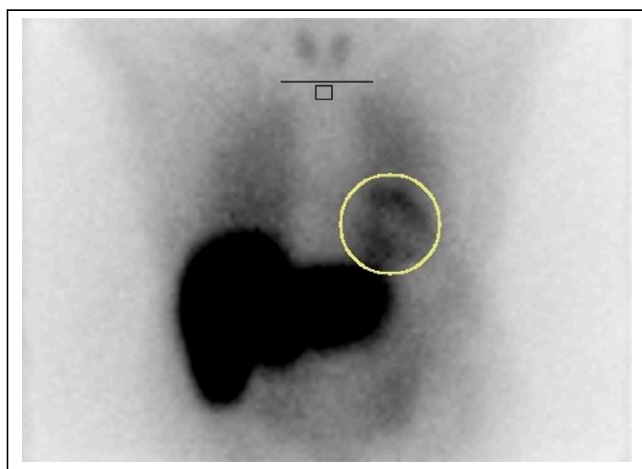


FIGURE 6. Example of ¹²³I-MIBG ROIs drawn for HMR calculation. Horizontal black line indicates location of clavicular heads, below which there is freehand rectangle for mediastinal background ROI (our technologists freehand draw these rectangles). Yellow circle encloses myocardial uptake.

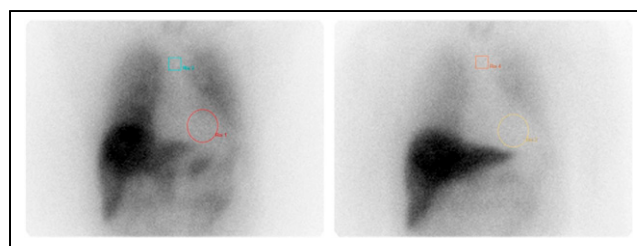


FIGURE 7. Example of early (15 min) (A) and delayed (4 h) (B) images for ¹²³I-MIBG scan demonstrating abnormal increased WR of 42.45%.

INTERPRETATION

¹²³I-MIBG interpretation includes qualitative, semiquantitative, and quantitative methods. Planar imaging uses qualitative and quantitative analysis, whereas SPECT imaging uses semiquantitative techniques. Early (15 min) and delayed (4 h) imaging should be evaluated qualitatively for myocardial uptake relative to the mediastinum and quantitatively for the HMR and WR. Normal delayed HMR ranges from 1.9 to 3.0, whereas WR varies between 21% and 37%, though values depend on physiologic and technical factors (31,49,50). Age, sex, cardiac function, and activity level impact physiologic variability, with HMR decreasing and WR increasing with age (3). Technical factors include ROI placement, administered activity, ¹²³I-MIBG-specific activity, and image acquisition settings (e.g., collimation, acquisition time) (3,5,31,51).

SPECT imaging uses a summed segmental approach, similar to perfusion imaging, but regional uptake differences create interpretation challenges, especially in older patients and men (3,31,48,52). Athletes may show lower inferior wall uptake due to increased vagal tone (53). Additionally, attenuation artifacts and absent myocardial uptake can affect SPECT accuracy (5,31).

Despite these variations, ¹²³I-MIBG remains a valuable tool for assessing sympathetic denervation and cardiac dysautonomia across multiple pathologies (3,5,31,54). Our institution has established HMR and WR thresholds based on data from the largest studies in the literature (Table 4) (32,46,48,55–60).

CHARACTERIZING CARDIAC AUTONOMIC DYSFUNCTION WITH ¹²³I-MIBG

Disruption of cardiac neural networks through intrinsic and extrinsic mechanisms results in autonomy dysfunction, which can be characterized with ¹²³I-MIBG imaging. We

will now discuss studies that demonstrate the utility of ¹²³I-MIBG scans in the previously described disorders.

Intrinsic Mechanisms

Dysautonomia. Among the causes of cardiac dysautonomia, ¹²³I-MIBG imaging has been used to assess cardiac dysautonomia in postural orthostatic tachycardia syndrome (POTS). Haensch et al. studied 20 patients with POTS using ¹²³I-MIBG SPECT imaging, comparing HMR with a normal threshold of more than 1.70 (61). Four patients with POTS showed significantly reduced uptake (mean HMR, 1.22 ± 0.08) compared with control patients with incidental tumors (mean HMR, 1.86 ± 0.18). The authors noted limitations, including the young age of participants, lack of age-matched controls, and variability in sympathetic cardiac denervation among POTS patients (61).

Amyloidosis. ¹²³I-MIBG imaging detects sympathetic denervation in cardiac amyloidosis, showing reduced HMR values below 1.60 at 4 h (13). Lower HMR predicts higher mortality, with a 42% 5-y all-cause mortality rate for values under 1.60, compared with 7% for those 1.60 or greater (13,62). All forms of cardiac amyloidosis (immunoglobulin light chain amyloidosis, hereditary ATTR, and wild-type ATTR) show reduced HMR (13,14). Although ¹²³I-MIBG cannot distinguish amyloid subtypes unlike amyloid PET imaging or bone scintigraphy, studies suggest it may detect cardiac involvement earlier than ^{99m}Tc-PYP can (12,63). In a study of 75 hereditary ATTR patients, 65% had cardiac denervation on ¹²³I-MIBG (HMR < 1.85), whereas only 39% showed abnormal ^{99m}Tc-PYP uptake (63). Notably, 29% of ^{99m}Tc-PYP-negative patients had abnormal ¹²³I-MIBG HMR, correlating with echocardiogram results, indicating that ¹²³I-MIBG may detect early cardiac involvement.

Diabetes Mellitus. Diabetes commonly causes cardiac dysautonomia because of sympathetic nerve damage, detectable with ¹²³I-MIBG imaging, especially using SPECT and

TABLE 4

Large Clinical Trials and Cohort Studies Using ¹²³I-MIBG for Heart Failure Prognostication and PD or DLB Diagnosis

Indication	Study	Type of study	Year	Study patients	Delayed time	Delayed HMR threshold or mean ± SD	WR threshold or mean ± SD
Heart failure	Seo et al.	Single center	2022	148	3.3 h	1.9	
	Nakata et al.	Multicenter	2013	1322	3–4 h	1.68	43%
	Doi et al.	Single center	2012	468	4 h	1.57 and 1.50 ± 0.36	41.3% ± 9.8%
	Jacobson et al.	Multicenter	2010	961	3 h 50 min	1.6 and 1.39 ± 0.18	41.8% ± 17.3%
	Nakata et al.	Single center	1998	414	3–4 h	1.74 and 1.56 ± 0.36	
PD or DLB	Odagiri et al.	Single center	2016	54	3 h	1.59 ± 0.34 for PD/1.31 ± 0.21 for DLB	
	Oka et al.	Single center	2011	110	3–4 h	1.58 ± 0.43	
	Kashihara et al.	Single center	2006	188	4 h	1.37 ± 0.27 for PD/1.47 ± 0.37 for DLB	
	Nagayama et al.	Single center	2005	391	4 h	1.38 ± 0.29 for PD/1.17 ± 0.06 for DLB	

Variety of delayed times were used, with 4 h being most common. Various thresholds and mean values for delayed HMR and WR were used or discovered. 1.6 delayed HMR threshold used in ADMIRE-HF trial does tend to fit many trial thresholds and mean values (32,46,48,55–60).

left ventricular segmental analysis (3,18,19). Langer et al. compared ^{123}I -MIBG and $^{99\text{m}}\text{Tc}$ -sestamibi scans in 65 asymptomatic diabetic patients and 23 controls, assessing segmental uptake (0 = normal to 4 = no uptake) and clinical autonomic dysfunction (19). Diabetic patients showed reduced ^{123}I -MIBG uptake in all segments except the septum compared with controls, with more severe reductions in those with clinical dysautonomia. Silent ischemic areas also exhibited greater uptake reduction because of neuronal ischemia. Nagamachi et al. studied 144 patients with type 2 diabetes and found that an HMR less than 1.7 independently predicted long-term mortality and, when combined with documented autonomic neuropathy, predicted cardiac-related death (18). Although ^{123}I -MIBG imaging shows diagnostic and prognostic promise in diabetes, further research is needed.

Parkinsonian Syndromes. PD causes degeneration of postganglionic sympathetic cardiac nerves, leading to cardiac dysautonomia detectable with ^{123}I -MIBG imaging (22,23,64). Japanese researchers first observed reduced HMR in PD patients (65–67). Satoh et al. found significantly lower HMR (<1.50) and higher WRs (>0.4) in 35 patients with PD compared with 24 controls (HMR, \sim 2.0; WR, <0.35), also confirming that anti-PD medications do not improve ^{123}I -MIBG uptake (66).

Unlike PD, MSA and progressive supranuclear palsy preserve postganglionic cardiac innervation (23,64,68), Sakuramoto et al. demonstrated 100% and 90% specificity in distinguishing PD from MSA and progressive supranuclear palsy using ^{123}I -MIBG (23). Eckhardt et al. also found significantly lower HMR in PD (1.18) than in MSA (1.79), making ^{123}I -MIBG a valuable tool for differentiating Parkinsonian syndromes with similar neurologic symptoms (68).

DLB, another Parkinsonian syndrome, also shows reduced cardiac ^{123}I -MIBG uptake, distinguishing it from Alzheimer dementia (69–71). Watanabe et al. found a median HMR of 1.2 in patients with DLB versus 2.4 in patients with Alzheimer and in controls (71). Manabe et al. further confirmed significantly lower HMR in DLB compared with non-DLB dementias, with an area under the curve of 0.879 for a 2.23 HMR cutoff, reinforcing ^{123}I -MIBG as a diagnostic tool for differentiating DLB from other dementias (70). These results demonstrate the utility of ^{123}I -MIBG scans as an additional tool for diagnostic differentiation of DLB from other dementias.

Extrinsic Mechanisms

Heart Failure. Chronic left ventricular heart failure leads to reduced presynaptic ^{123}I -MIBG uptake and increased washout, providing valuable prognostic and management insights (2,5,29,32,47,50,72). Merlet et al. studied 112 patients with heart failure (New York Heart Association class II–IV, left ventricular ejection fraction < 40%) over a mean of 27 mo, identifying low HMR and left ventricular ejection fraction as independent mortality predictors (72). Patients had an average delayed HMR of 1.23 ± 0.19 , compared with a normal HMR of 1.95 ± 0.31 . Nakata et al.

followed 414 patients (42% with symptomatic heart failure) for an average of 22 mo, finding that an HMR of no more than 1.74 independently predicted cardiac death due to heart failure, sudden cardiac death, or myocardial infarction (59). The ADMIRE-HF study (961 patients, New York Heart Association class II/III, left ventricular ejection fraction \leq 35%) confirmed that an HMR of less than 1.60 was linked to higher mortality and cardiac event rates over 2 y, with a hazard ratio of 0.36 (32). A pooled analysis of 1,322 patients with heart failure identified an HMR of 1.68 or less and a WR greater than 43% as predictors of lower overall survival in New York Heart Association class I–IV patients (60). Patients were also categorized into low-risk (>2.10), intermediate-risk (1.40–2.10), and high risk (<1.40) groups, with delayed HMR independently predicting all-cause mortality (hazard ratio, 0.85). ^{123}I -MIBG imaging has also demonstrated treatment benefits, showing improved uptake and HMR ratios with β -blockers, angiotensin-converting enzyme inhibitors, amiodarone, left ventricular assist devices, and cardiac resynchronization therapy (3). These findings support the role of ^{123}I -MIBG in prognosis and heart failure management.

Myocardial Ischemia or Infarction. Myocardial ischemia and infarction damage both postsynaptic myocytes and postganglionic sympathetic neurons, detectable with ^{123}I -MIBG imaging (3). Tomoda et al. compared ^{123}I -MIBG and ^{201}Tl Cl imaging in 8 patients with myocardial infarction and 12 with unstable angina, finding ^{123}I -MIBG uptake defects in all patients with myocardial infarction (8/8) and in 7 of 12 patients with angina, whereas ^{201}Tl Cl defects were present in only 4 of 8 patients with myocardial infarction and none of the patients with angina (73). This suggests ^{123}I -MIBG may be more sensitive for ischemia detection than older perfusion agents. In 30 asymptomatic individuals with a strong family history of early coronary artery disease, reduced delayed ^{123}I -MIBG uptake correlated with coronary artery stenosis despite normal $^{99\text{m}}\text{Tc}$ -sestamibi perfusion (74). Additionally, ^{123}I -MIBG defects align with left ventricular remodeling postmyocardial infarction, reinforcing its diagnostic and prognostic role in ischemic heart disease, even in asymptomatic patients (75).

CONCLUSION

^{123}I -MIBG imaging is a valuable tool for assessing cardiac sympathetic innervation in conditions such as heart failure, ischemic heart disease, PD, and DLB. However, the lack of standardized protocols has led to variability in image acquisition and interpretation across institutions, limiting universally accepted benchmarks. To improve consistency, we propose a simplified protocol based on EANM guidelines and the ADMIRE-HF trial, standardizing patient preparation, image acquisition, and interpretation using metrics such as HMR. A uniform approach will enhance diagnostic accuracy and improve the management of cardiac sympathetic dysfunction.

DISCLOSURE

The views expressed in this article are those of the authors and do not reflect the official policy of the Uniformed Services University, Department of Army/Navy/Air Force, Department of Defense, or U.S. Government. The authors used ChatGPT-4o (OpenAI, 2024) to provide editorial suggestions and text refinement for clarity and conciseness during the revision process. All final content, interpretations, and conclusions are the responsibility of the authors. No other potential conflict of interest relevant to this article was reported.

ACKNOWLEDGMENTS

We thank Prince Anbiah, CNMT, CT(NM), at Walter Reed National Military Medical Center for his help in figure generation. We want to thank Mary Beth Farrell, CNMT, at Molecular Imaging Services and Aspen University for her helpful edits to the article.

KEY POINTS

QUESTION: Can a standardized protocol for cardiac ^{123}I -MIBG imaging be established to improve the detection, characterization, and prognostic assessment of sympathetic dysfunction across various cardiac conditions?

PERTINENT FINDINGS: Cardiac sympathetic dysfunction arises from intrinsic (e.g., dysautonomias, amyloidosis, Parkinsonian syndromes) and extrinsic (e.g., heart failure, myocardial ischemia) mechanisms. Standardized ^{123}I -MIBG imaging protocols, incorporating qualitative, semiquantitative, and quantitative methods (e.g., HMR and WR), can accurately assess disease severity and predict outcomes. Variability in image acquisition and interpretation has limited universal benchmarks, highlighting the need for a simplified and consistent imaging approach.

IMPLICATIONS FOR PATIENT CARE: Implementing a standardized cardiac ^{123}I -MIBG protocol will improve diagnostic accuracy, enhance prognostic evaluation, and ensure consistency across institutions. This will lead to better clinical decision-making, optimized treatment strategies, and improved patient outcomes in those with cardiac autonomic dysfunction.

REFERENCES

- Goldberger JJ, Arora R, Buckley U, Shivkumar K. Autonomic nervous system dysfunction. *J Am Coll Cardiol*. 2019;73:1189–1206.
- Jacobson AF, Narula J. Introduction to cardiac neuronal imaging: a clinical perspective. *J Nucl Med*. 2015;56(suppl 4):3S–6S.
- Chirumamilla A, Travin MI. Cardiac applications of ^{123}I -MIBG imaging. *Semin Nucl Med*. 2011;41:374–387.
- Zhang DY, Anderson AS. The sympathetic nervous system and heart failure. *Cardiol Clin*. 2014;32:33–45.
- Christensen TE, Kjaer A, Hasbak P. The clinical value of cardiac sympathetic imaging in heart failure. *Clin Physiol Funct Imaging*. 2014;34:178–182.
- Patel AD, Iskandrian AE. MIBG imaging. *J Nucl Cardiol*. 2002;9:75–94.
- Motiejunaite J, Amar L, Vidal-Petiot E. Adrenergic receptors and cardiovascular effects of catecholamines. *Ann Endocrinol (Paris)*. 2021;82:193–197.
- Xavier de Brito AS, Bronchtein AI, Schaustz EB, et al. Value of ^{123}I -MIBG SPECT for the assessment of dysautonomia in patients with long COVID. *Int J Cardiol Heart Vasc*. 2024;52:101413.
- Rafanelli M, Walsh K, Hamdan MH, Buyan-Dent L. Autonomic dysfunction: diagnosis and management. In: Dekosky ST, Asthana S, eds. *Handbook of Clinical Neurology*. Vol 167. Elsevier; 2019:123–137.
- Dysautonomia: Malfunctions in Your Body's Automatic Functions. Cleveland Clinic website. <https://my.clevelandclinic.org/health/diseases/6004-dysautonomia>. Updated September 11, 2023. Accessed September 2, 2024.
- Dineen J, Freeman R. Autonomic neuropathy. *Semin Neurol*. 2015;35:458–468.
- Embry-Dierson M, Farrell MB, Schockling E, Warren J, Jerome S. Cardiac amyloidosis imaging, part 1: amyloidosis etiology and image acquisition. *J Nucl Med Technol*. 2023;51:83–89.
- Slart RHJA, Glaudemans AWJM, Hazenberg BPC, Noordzij W. Imaging cardiac innervation in amyloidosis. *J Nucl Cardiol*. 2019;26:174–187.
- Lekakis J, Dimopoulos MA, Prassopoulos V, et al. Myocardial adrenergic denervation in patients with primary (AL) amyloidosis. *Amyloid*. 2003;10:117–120.
- Dyrberg T, Benn J, Christiansen JS, Hilsted J, Nerup J. Prevalence of diabetic autonomic neuropathy measured by simple bedside tests. *Diabetologia*. 1981;20:190–194.
- Ewing DJ, Campbell IW, Clarke BF. The natural history of diabetic autonomic neuropathy. *Q J Med*. 1980;49:95–108.
- Hattori N, Tamaki N, Hayashi T, et al. Regional abnormality of iodine-123-MIBG in diabetic hearts. *J Nucl Med*. 1996;37:1985–1990.
- Nagamachi S, Fujita S, Nishii R, et al. Prognostic value of cardiac I-123 metaiodobenzylguanidine imaging in patients with non-insulin-dependent diabetes mellitus. *J Nucl Cardiol*. 2006;13:34–42.
- Langer A, Freeman MR, Josse RG, Armstrong PW. Metaiodobenzylguanidine imaging in diabetes mellitus: assessment of cardiac sympathetic denervation and its relation to autonomic dysfunction and silent myocardial ischemia. *J Am Coll Cardiol*. 1995;25:610–618.
- Paolini Paoletti F, Gaetani L, Parnetti L. Molecular profiling in Parkinsonian syndromes: CSF biomarkers. *Clin Chim Acta*. 2020;506:55–66.
- Goldstein DS. Dysautonomia in Parkinson's disease: neurocardiological abnormalities. *Lancet Neurol*. 2003;2:669–676.
- Orimo S, Yogo M, Nakamura T, Suzuki M, Watanabe H. ^{123}I -metaiodobenzylguanidine (MIBG) cardiac scintigraphy in α -synucleinopathies. *Ageing Res Rev*. 2016;30:122–133.
- Sakuramoto H, Fujita H, Suzuki K, et al. Combination of midbrain-to-pontine ratio and cardiac MIBG scintigraphy to differentiate Parkinson's disease from multiple system atrophy and progressive supranuclear palsy. *Clin Park Relat Disord*. 2019;2:20–24.
- Hartikainen J, Mustonen J, Kuikka J, Vanninen E, Kettunen R. Cardiac sympathetic denervation in patients with coronary artery disease without previous myocardial infarction. *Am J Cardiol*. 1997;80:273–277.
- Wieland DM, Wu J L, Brown LE, Mangner TJ, Swanson DP, Beierwaltes WH. Radiolabeled adrenergic neuron-blocking agents: adrenomedullary imaging with [^{131}I]iodobenzylguanidine. *J Nucl Med*. 1980;21:349–353.
- Sisson JC, Frager MS, Valk TW, et al. Scintigraphic localization of pheochromocytoma. *N Engl J Med*. 1981;305:12–17.
- Moll LV, McEwan AJ, Shapiro B, et al. Iodine-131 MIBG scintigraphy of neuroendocrine tumors other than pheochromocytoma and neuroblastoma. *J Nucl Med*. 1987;28:979–988.
- Nakajo M, Shapiro B, Copp J, et al. The normal and abnormal distribution of the adrenomedullary imaging agent m-[^{131}I]iodobenzylguanidine (I-131 MIBG) in man: evaluation by scintigraphy. *J Nucl Med*. 1983;24:672–682.
- Carrió I, Cowie MR, Yamazaki J, Udelson J, Camici PG. Cardiac sympathetic imaging with mIBG in heart failure. *JACC Cardiovasc Imaging*. 2010;3:92–100.
- Flotats A, Carrió I, Agostini D, et al.; European Council of Nuclear Cardiology. Proposal for standardization of ^{123}I -metaiodobenzylguanidine (MIBG) cardiac sympathetic imaging by the EANM Cardiovascular Committee and the European Council of Nuclear Cardiology. *Eur J Nucl Med Mol Imaging*. 2010;37:1802–1812.
- Nakajima K, Nakata T. Cardiac ^{123}I -MIBG imaging for clinical decision making: 22-year experience in Japan. *J Nucl Med*. 2015;56(suppl 4):11S–19S.
- Jacobson AF, Senior R, Cerqueira MD, et al.; ADMIRE-HF Investigators. Myocardial iodine-123 meta-iodobenzylguanidine imaging and cardiac events in heart failure. *J Am Coll Cardiol*. 2010;55:2212–2221.
- Agostini D, Carrió I, Verberne HJ. How to use myocardial ^{123}I -MIBG scintigraphy in chronic heart failure. *Eur J Nucl Med Mol Imaging*. 2009;36:555–559.
- Agostini D, Ananthasubramanian K, Chandna H, et al.; ADMIRE-HF investigators. Prognostic usefulness of planar ^{123}I -MIBG scintigraphic images of myocardial sympathetic innervation in congestive heart failure: follow-up data from ADMIRE-HF. *J Nucl Cardiol*. 2021;28:1490–1503.
- ADREVIEW- iobenguane i-123 injection. DailyMed website. <https://dailymed.nlm.nih.gov/dailymed/lookup.cfm?setid=c89d3ecc-4f4c-4566-8808-79152344194d>. Updated January 10, 2024. Accessed October 14, 2024.
- Bombardieri E, Giammarile F, Aktolun C, et al.; European Association for Nuclear Medicine. $^{131}\text{I}/^{123}\text{I}$ -metaiodobenzylguanidine (mIBG) scintigraphy: procedure guidelines for tumour imaging. *Eur J Nucl Med Mol Imaging*. 2010;37:2436–2446.

37. Vickle SSV, Thompson RC. ^{123}I -MIBG imaging: patient preparation and technologist's role. *J Nucl Med Technol*. 2015;43:82–86.
38. Yamashina S, Yamazaki JI. Neuronal imaging using SPECT. *Eur J Nucl Med Mol Imaging*. 2007;34(suppl 1):62–73.
39. Solanki KK, Bomanji J, Moyes J, Mather SJ, Trainer PJ, Britton KE. A pharmacological guide to medicines which interfere with the biodistribution of radiolabelled meta-iodobenzylguanidine (MIBG). *Nucl Med Commun*. 1992;13:513–521.
40. Taieb D, Timmers HJ, Hindie E, et al.; European Association of Nuclear Medicine. EANM 2012 guidelines for radionuclide imaging of pheochromocytoma and paraganglioma. *Eur J Nucl Med Mol Imaging*. 2012;39:1977–1995.
41. Bar-Sever Z, Biassoni L, Shulkin B, et al. Guidelines on nuclear medicine imaging in neuroblastoma. *Eur J Nucl Med Mol Imaging*. 2018;45:2009–2024.
42. Gelfand MJ, Parisi MT, Treves ST; Pediatric Nuclear Medicine Dose Reduction Workgroup. Pediatric radiopharmaceutical administered doses: 2010 North American Consensus Guidelines. *J Nucl Med*. 2011;52:318–322.
43. Lassmann M, Treves ST; For the EANM/SNMMI Paediatric Dosage Harmonization Working Group. Paediatric radiopharmaceutical administration: harmonization of the 2007 EANM paediatric dosage card (version 1.5.2008) and the 2010 North American consensus guidelines. *Eur J Nucl Med Mol Imaging*. 2014;41:1036–1041.
44. Wakabayashi T, Nakata T, Hashimoto A, et al. Assessment of underlying etiology and cardiac sympathetic innervation to identify patients at high risk of cardiac death. *J Nucl Med*. 2001;42:1757–1767.
45. Somsen GA, Verberne HJ, Fleury E, Righetti A. Normal values and within-subject variability of cardiac I-123 MIBG scintigraphy in healthy individuals: implications for clinical studies. *J Nucl Cardiol*. 2004;11:126–133.
46. Odagiri H, Baba T, Nishio Y, et al. On the utility of MIBG SPECT/CT in evaluating cardiac sympathetic dysfunction in Lewy body diseases. *PLoS One*. 2016;11:e0152746.
47. Dimitriu-Leen AC, Scholte AJHA, Jacobson AF. ^{123}I -MIBG SPECT for evaluation of patients with heart failure. *J Nucl Med*. 2015;56(suppl 4):25S–30S.
48. Seo M, Yamada T, Tamaki S, et al. Prognostic significance of cardiac ^{123}I -MIBG SPECT imaging in heart failure patients with preserved ejection fraction. *JACC Cardiovasc Imaging*. 2022;15:655–668.
49. Travin MI. Current clinical applications and next steps for cardiac innervation imaging. *Curr Cardiol Rep*. 2017;19:1.
50. Hattori N, Schwaiger M. Metaiodobenzylguanidine scintigraphy of the heart: what have we learnt clinically? *Eur J Nucl Med*. 2000;27:1–6.
51. Nakajima K, Okuda K, Yoshimura M, et al. Multicenter cross-calibration of I-123 metaiodobenzylguanidine heart-to-mediastinum ratios to overcome camera-collimator variations. *J Nucl Cardiol*. 2014;21:970–978.
52. Tsuchimochi S, Tamaki N, Tadamura E, et al. Age and gender differences in normal myocardial adrenergic neuronal function evaluated by iodine-123-MIBG imaging. *J Nucl Med*. 1995;36:969–974.
53. Estorch M, Serra-Grima R, Flotats A, et al. Myocardial sympathetic innervation in the athlete's sinus bradycardia: is there selective inferior myocardial wall denervation? *J Nucl Cardiol*. 2000;7:354–358.
54. Sciammarella MG, Gerson M, Buxton AE, et al. ASNC/SNMMI model coverage policy: myocardial sympathetic innervation imaging—iodine-123 meta-iodobenzylguanidine (^{123}I -mIBG). *J Nucl Cardiol*. 2015;22:804–811.
55. Doi T, Nakata T, Hashimoto A, et al. Cardiac mortality assessment improved by evaluation of cardiac sympathetic nerve activity in combination with hemoglobin and kidney function in chronic heart failure patients. *J Nucl Med*. 2012;53:731–740.
56. Oka H, Toyoda C, Yogo M, Mochio S. Reduced cardiac ^{123}I -MIBG uptake reflects cardiac sympathetic dysfunction in de novo Parkinson's disease. *J Neural Transm (Vienna)*. 2011;118:1323–1327.
57. Kashiwara K, Ohno M, Kawada S, Okumura Y. Reduced cardiac uptake and enhanced washout of ^{123}I -MIBG in pure autonomic failure occurs conjointly with Parkinson's disease and dementia with Lewy bodies. *J Nucl Med*. 2006;47:1099–1101.
58. Nagayama H, Hamamoto M, Ueda M, Nagashima J, Katayama Y. Reliability of MIBG myocardial scintigraphy in the diagnosis of Parkinson's disease. *J Neurol Neurosurg Psychiatry*. 2005;76:249–251.
59. Nakata T, Miyamoto K, Doi A, et al. Cardiac death prediction and impaired cardiac sympathetic innervation assessed by MIBG in patients with failing and nonfailing hearts. *J Nucl Cardiol*. 1998;5:579–590.
60. Nakata T, Nakajima K, Yamashina S, et al. A pooled analysis of multicenter cohort studies of ^{123}I -mIBG imaging of sympathetic innervation for assessment of long-term prognosis in heart failure. *JACC Cardiovasc Imaging*. 2013;6:772–784.
61. Haensch CA, Lerch H, Schlemmer H, Jigalin A, Isenmann S. Cardiac neurotransmission imaging with ^{123}I -meta-iodobenzylguanidine in postural tachycardia syndrome. *J Neurol Neurosurg Psychiatry*. 2010;81:339–343.
62. Coutinho MCA, Cortez-Dias N, Cantinho G, et al. Reduced myocardial 123-iodine metaiodobenzylguanidine uptake. *Circ Cardiovasc Imaging*. 2013;6:627–636.
63. Piekarski E, Chequer R, Algarrondo V, et al. Cardiac denervation evidenced by MIBG occurs earlier than amyloid deposits detection by diphosphonate scintigraphy in TTR mutation carriers. *Eur J Nucl Med Mol Imaging*. 2018;45:1108–1118.
64. Treglia G, Stefanelli A, Cason E, Cocciolillo F, Di Giuda D, Giordano A. Diagnostic performance of iodine-123-metaiodobenzylguanidine scintigraphy in differential diagnosis between Parkinson's disease and multiple-system atrophy: a systematic review and a meta-analysis. *Clin Neurol Neurosurg*. 2011;113:823–829.
65. Satoh A, Serita T, Tsujihata M. Total defect of metaiodobenzylguanidine (MIBG) imaging on heart in Parkinson's disease: assessment of cardiac sympathetic denervation [in Japanese]. *Nihon Rinsho*. 1997;55:202–206.
66. Satoh A, Serita T, Seto M, et al. Loss of ^{123}I -MIBG uptake by the heart in Parkinson's disease: assessment of cardiac sympathetic denervation and diagnostic value. *J Nucl Med*. 1999;40:371–375.
67. Hakusui S, Yasuda T, Yanagi T, Takahashi A, Hasegawa Y, Inoue M. ^{123}I -MIBG myocardial scintigraphical analysis in patients with and without autonomic disorder [in Japanese]. *Rinsho Shinkeigaku*. 1994;34:402–404.
68. Eckhardt C, Krismer F, Donnemiller E, et al. Cardiac sympathetic innervation in Parkinson's disease versus multiple system atrophy. *Clin Auton Res*. 2022;32:103–114.
69. Yoshita M, Taki J, Yamada M. A clinical role for [^{123}I]MIBG myocardial scintigraphy in the distinction between dementia of the Alzheimer's-type and dementia with Lewy bodies. *J Neurol Neurosurg Psychiatry*. 2001;71:583–588.
70. Manabe Y, Inui Y, Toyama H, Kosaka K. ^{123}I -metaiodobenzylguanidine myocardial scintigraphy with early images alone is useful for the differential diagnosis of dementia with Lewy bodies. *Psychiatry Res Neuroimaging*. 2017;261:75–79.
71. Watanabe H, Ieda T, Katayama T, et al. Cardiac ^{123}I -meta-iodobenzylguanidine (MIBG) uptake in dementia with Lewy bodies: comparison with Alzheimer's disease. *J Neurol Neurosurg Psychiatry*. 2001;70:781–783.
72. Merlet P, Valette H, Dubois-Randé JL, et al. Prognostic value of cardiac metaiodobenzylguanidine imaging in patients with heart failure. *J Nucl Med*. 1992;33:471–477.
73. Tomoda H, Yoshioka K, Shiina Y, Tagawa R, Ide M, Suzuki Y. Regional sympathetic denervation detected by iodine 123 metaiodobenzylguanidine in non-Q-wave myocardial infarction and unstable angina. *Am Heart J*. 1994;128:452–458.
74. Simula S, Vanninen E, Viitanen L, et al. Cardiac adrenergic innervation is affected in asymptomatic subjects with very early stage of coronary artery disease. *J Nucl Med*. 2002;43:1–7.
75. Sakata K, Mochizuki M, Yoshida H, et al. Cardiac sympathetic dysfunction contributes to left ventricular remodeling after acute myocardial infarction. *Eur J Nucl Med*. 2000;27:1641–1649.